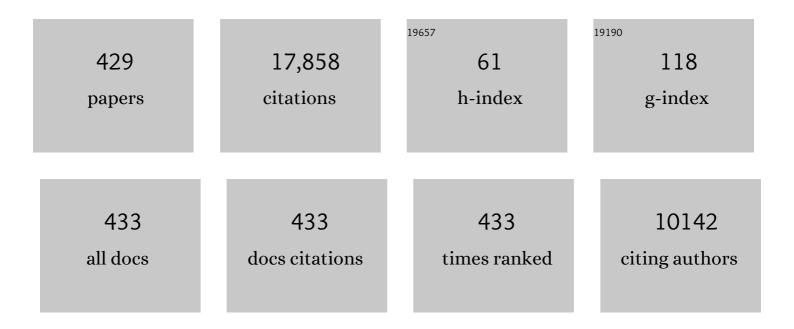
Ge Wang

List of Publications by Year in descending order

Source: https://exaly.com/author-pdf/1681508/publications.pdf Version: 2024-02-01



#	Article	IF	CITATIONS
1	Low-Dose CT With a Residual Encoder-Decoder Convolutional Neural Network. IEEE Transactions on Medical Imaging, 2017, 36, 2524-2535.	8.9	1,089
2	Low-Dose CT Image Denoising Using a Generative Adversarial Network With Wasserstein Distance and Perceptual Loss. IEEE Transactions on Medical Imaging, 2018, 37, 1348-1357.	8.9	983
3	aLow-dose CT via convolutional neural network. Biomedical Optics Express, 2017, 8, 679.	2.9	549
4	Low-Dose X-ray CT Reconstruction via Dictionary Learning. IEEE Transactions on Medical Imaging, 2012, 31, 1682-1697.	8.9	494
5	Compressed sensing based interior tomography. Physics in Medicine and Biology, 2009, 54, 2791-2805.	3.0	458
6	Image Reconstruction is a New Frontier of Machine Learning. IEEE Transactions on Medical Imaging, 2018, 37, 1289-1296.	8.9	366
7	A Perspective on Deep Imaging. IEEE Access, 2016, 4, 8914-8924.	4.2	340
8	Iterative deblurring for CT metal artifact reduction. IEEE Transactions on Medical Imaging, 1996, 15, 657-664.	8.9	329
9	3-D Convolutional Encoder-Decoder Network for Low-Dose CT via Transfer Learning From a 2-D Trained Network. IEEE Transactions on Medical Imaging, 2018, 37, 1522-1534.	8.9	303
10	Practical reconstruction method for bioluminescence tomography. Optics Express, 2005, 13, 6756.	3.4	299
11	CT Super-Resolution GAN Constrained by the Identical, Residual, and Cycle Learning Ensemble (GAN-CIRCLE). IEEE Transactions on Medical Imaging, 2020, 39, 188-203.	8.9	289
12	LEARN: Learned Experts' Assessment-Based Reconstruction Network for Sparse-Data CT. IEEE Transactions on Medical Imaging, 2018, 37, 1333-1347.	8.9	269
13	Competitive performance of a modularized deep neural network compared to commercial algorithms for low-dose CT image reconstruction. Nature Machine Intelligence, 2019, 1, 269-276.	16.0	256
14	Uniqueness theorems in bioluminescence tomography. Medical Physics, 2004, 31, 2289-2299.	3.0	253
15	A Roadmap for Foundational Research on Artificial Intelligence in Medical Imaging: From the 2018 NIH/RSNA/ACR/The Academy Workshop. Radiology, 2019, 291, 781-791.	7.3	241
16	Deep learning for tomographic image reconstruction. Nature Machine Intelligence, 2020, 2, 737-748.	16.0	233
17	An outlook on xâ€ray CT research and development. Medical Physics, 2008, 35, 1051-1064.	3.0	218
18	Convergence studies on iterative algorithms for image reconstruction. IEEE Transactions on Medical Imaging, 2003, 22, 569-579.	8.9	198

#	Article	IF	CITATIONS
19	Multi-energy CT based on a prior rank, intensity and sparsity model (PRISM). Inverse Problems, 2011, 27, 115012.	2.0	191
20	On Interpretability of Artificial Neural Networks: A Survey. IEEE Transactions on Radiation and Plasma Medical Sciences, 2021, 5, 741-760.	3.7	188
21	Convergence of the simultaneous algebraic reconstruction technique (SART). IEEE Transactions on Image Processing, 2003, 12, 957-961.	9.8	187
22	A soft-threshold filtering approach for reconstruction from a limited number of projections. Physics in Medicine and Biology, 2010, 55, 3905-3916.	3.0	176
23	A multilevel adaptive finite element algorithm for bioluminescence tomography. Optics Express, 2006, 14, 8211.	3.4	172
24	Structurally-Sensitive Multi-Scale Deep Neural Network for Low-Dose CT Denoising. IEEE Access, 2018, 6, 41839-41855.	4.2	169
25	In vivo mouse studies with bioluminescence tomography. Optics Express, 2006, 14, 7801.	3.4	167
26	Metal Artifact Reduction in CT: Where Are We After Four Decades?. IEEE Access, 2016, 4, 5826-5849.	4.2	164
27	Iterative X-ray Cone-Beam Tomography for Metal Artifact Reduction and Local Region Reconstruction. Microscopy and Microanalysis, 1999, 5, 58-65.	0.4	136
28	A General Local Reconstruction Approach Based on a Truncated Hilbert Transform. International Journal of Biomedical Imaging, 2007, 2007, 1-8.	3.9	136
29	Fast iterative algorithm for metal artifact reduction in X-ray CT. Academic Radiology, 2000, 7, 607-614.	2.5	133
30	Tensor-Based Dictionary Learning for Spectral CT Reconstruction. IEEE Transactions on Medical Imaging, 2017, 36, 142-154.	8.9	131
31	A mouse optical simulation environment (MOSE) to investigate bioluminescent phenomena in the living mouse with the monte carlo method1. Academic Radiology, 2004, 11, 1029-1038.	2.5	126
32	Recycling mechanisms and policy suggestions for spent electric vehicles' power battery -A case of Beijing. Journal of Cleaner Production, 2018, 186, 388-406.	9.3	126
33	A finite-element-based reconstruction method for 3D fluorescence tomography. Optics Express, 2005, 13, 9847.	3.4	124
34	High-order total variation minimization for interior tomography. Inverse Problems, 2010, 26, 035013.	2.0	115
35	Metal artifacts in computed tomography for radiation therapy planning: dosimetric effects and impact of metal artifact reduction. Physics in Medicine and Biology, 2017, 62, R49-R80.	3.0	104
36	Assessment of morphometry of pulmonary acini in mouse lungs by nondestructive imaging using multiscale microcomputed tomography. Proceedings of the National Academy of Sciences of the United States of America, 2012, 109, 17105-17110.	7.1	103

#	Article	IF	CITATIONS
37	Determining scientific impact using a collaboration index. Proceedings of the National Academy of Sciences of the United States of America, 2013, 110, 9680-9685.	7.1	102
38	DRONE: Dual-Domain Residual-based Optimization NEtwork for Sparse-View CT Reconstruction. IEEE Transactions on Medical Imaging, 2021, 40, 3002-3014.	8.9	101
39	Tensor-based dictionary learning for dynamic tomographic reconstruction. Physics in Medicine and Biology, 2015, 60, 2803-2818.	3.0	99
40	Few-view image reconstruction with dual dictionaries. Physics in Medicine and Biology, 2012, 57, 173-189.	3.0	98
41	X-ray micro-CT with a displaced detector array. Medical Physics, 2002, 29, 1634-1636.	3.0	95
42	A Segmentation-Based Method for Metal Artifact Reduction. Academic Radiology, 2007, 14, 495-504.	2.5	93
43	Substitution effect of renewable portfolio standards and renewable energy certificate trading for feed-in tariff. Applied Energy, 2018, 227, 426-435.	10.1	90
44	A general exact reconstruction for cone-beam CT via backprojection-filtration. IEEE Transactions on Medical Imaging, 2005, 24, 1190-1198.	8.9	89
45	Accuracy of facial soft tissue thickness measurements in personal computer-based multiplanar reconstructed computed tomographic images. Forensic Science International, 2005, 155, 28-34.	2.2	88
46	Multi-Contrast Super-Resolution MRI Through a Progressive Network. IEEE Transactions on Medical Imaging, 2020, 39, 2738-2749.	8.9	88
47	Spectral CT Reconstruction With Image Sparsity and Spectral Mean. IEEE Transactions on Computational Imaging, 2016, 2, 510-523.	4.4	86
48	GI tract unraveling with curved cross sections. IEEE Transactions on Medical Imaging, 1998, 17, 318-322.	8.9	85
49	A review of photovoltaic poverty alleviation projects in China: Current status, challenge and policy recommendations. Renewable and Sustainable Energy Reviews, 2018, 94, 214-223.	16.4	85
50	Image Reconstruction for Hybrid True-Color Micro-CT. IEEE Transactions on Biomedical Engineering, 2012, 59, 1711-1719.	4.2	81
51	L_p regularization for early gate fluorescence molecular tomography. Optics Letters, 2014, 39, 4156.	3.3	78
52	Statistical Interior Tomography. IEEE Transactions on Medical Imaging, 2011, 30, 1116-1128.	8.9	77
53	Low-dose CT denoising with convolutional neural network. , 2017, , .		76
54	The meaning of interior tomography. Physics in Medicine and Biology, 2013, 58, R161-R186.	3.0	75

#	Article	IF	CITATIONS
55	Three-dimensional dental imaging by spiral CT. Oral Surgery Oral Medicine Oral Pathology Oral Radiology and Endodontics, 1997, 84, 561-570.	1.4	73
56	Quadratic Autoencoder (Q-AE) for Low-Dose CT Denoising. IEEE Transactions on Medical Imaging, 2020, 39, 2035-2050.	8.9	72
57	Data Consistency Based Rigid Motion Artifact Reduction in Fan-Beam CT. IEEE Transactions on Medical Imaging, 2007, 26, 249-260.	8.9	70
58	Spiral CT image deblurring for cochlear implantation. IEEE Transactions on Medical Imaging, 1998, 17, 251-262.	8.9	68
59	Ultra-low Dose Lung CT Perfusion Regularized by a Previous Scan. Academic Radiology, 2009, 16, 363-373.	2.5	68
60	The origin of intracellular structures in Ediacaran metazoan embryos. Geology, 2012, 40, 223-226.	4.4	68
61	The comprehensive imaging-based analysis of the lung. Academic Radiology, 2004, 11, 1370-1380.	2.5	67
62	Filtered backprojection formula for exact image reconstruction from cone-beam data along a general scanning curve. Medical Physics, 2004, 32, 42-48.	3.0	66
63	MRI Super-Resolution With Ensemble Learning and Complementary Priors. IEEE Transactions on Computational Imaging, 2020, 6, 615-624.	4.4	64
64	Blind deblurring of spiral CT images. IEEE Transactions on Medical Imaging, 2003, 22, 837-845.	8.9	61
65	Mathematical theory and numerical analysis of bioluminescence tomography. Inverse Problems, 2006, 22, 1659-1675.	2.0	61
66	Dual-dictionary learning-based iterative image reconstruction for spectral computed tomography application. Physics in Medicine and Biology, 2012, 57, 8217-8229.	3.0	60
67	A few-view reweighted sparsity hunting (FRESH) method for CT image reconstruction. Journal of X-Ray Science and Technology, 2013, 21, 161-176.	1.0	60
68	Supplemental analysis on compressed sensing based interior tomography. Physics in Medicine and Biology, 2009, 54, N425-N432.	3.0	59
69	The effect of pitch in multislice spiral/helical CT. Medical Physics, 1999, 26, 2648-2653.	3.0	58
70	Tissue-Specific Compartmental Analysis for Dynamic Contrast-Enhanced MR Imaging of Complex Tumors. IEEE Transactions on Medical Imaging, 2011, 30, 2044-2058.	8.9	58
71	Al-Based Reconstruction for Fast MRI—A Systematic Review and Meta-Analysis. Proceedings of the IEEE, 2022, 110, 224-245.	21.3	57
72	Optimization of Kâ€edge imaging with spectral CT. Medical Physics, 2012, 39, 6572-6579.	3.0	56

#	Article	IF	CITATIONS
73	Study on the impacts of natural gas supply cost on gas flow and infrastructure deployment in China. Applied Energy, 2016, 162, 1385-1398.	10.1	55
74	Molecular Optical Simulation Environment (MOSE): A Platform for the Simulation of Light Propagation in Turbid Media. PLoS ONE, 2013, 8, e61304.	2.5	53
75	Spectral CT Modeling and Reconstruction With Hybrid Detectors in Dynamic-Threshold-Based Counting and Integrating Modes. IEEE Transactions on Medical Imaging, 2015, 34, 716-728.	8.9	53
76	Study on the promotion impact of demand response on distributed PV penetration by using non-cooperative game theoretical analysis. Applied Energy, 2017, 185, 1869-1878.	10.1	52
77	Coordination of tradable carbon emission permits market and renewable electricity certificates market in China. Energy Economics, 2021, 93, 105038.	12.1	52
78	A unified framework for exact cone-beam reconstruction formulas. Medical Physics, 2005, 32, 1712-1721.	3.0	51
79	Stereological assessment of mouse lung parenchyma via nondestructive, multiscale micro-CT imaging validated by light microscopic histology. Journal of Applied Physiology, 2013, 114, 716-724.	2.5	51
80	Shape and margin-aware lung nodule classification in low-dose CT images via soft activation mapping. Medical Image Analysis, 2020, 60, 101628.	11.6	51
81	Multispectral Bioluminescence Tomography: Methodology and Simulation. International Journal of Biomedical Imaging, 2006, 2006, 1-7.	3.9	50
82	A Born-type approximation method for bioluminescence tomography. Medical Physics, 2006, 33, 679-686.	3.0	50
83	Approximate and exact cone-beam reconstruction with standard and non-standard spiral scanning. Physics in Medicine and Biology, 2007, 52, R1-R13.	3.0	49
84	Exact Interior Reconstruction with Cone-Beam CT. International Journal of Biomedical Imaging, 2007, 2007, 1-5.	3.9	49
85	A scheme for multisource interior tomography. Medical Physics, 2009, 36, 3575-3581.	3.0	49
86	Sart-Type Half-Threshold Filtering Approach for CT Reconstruction. IEEE Access, 2014, 2, 602-613.	4.2	49
87	A method of rapid quantification of patientâ€specific organ doses for CT using deepâ€learningâ€based multiâ€organ segmentation and CPUâ€accelerated Monte Carlo dose computing. Medical Physics, 2020, 47, 2526-2536.	3.0	49
88	Half-scan cone-beam CT fluoroscopy with multiple x-ray sources. Medical Physics, 2001, 28, 1466-1471.	3.0	48
89	Data consistency based translational motion artifact reduction in fan-beam CT. IEEE Transactions on Medical Imaging, 2006, 25, 792-803.	8.9	48
90	Efficient and equitable allocation of renewable portfolio standards targets among China's provinces. Energy Policy, 2019, 125, 170-180.	8.8	47

#	Article	IF	CITATIONS
91	Investment strategy for underground gas storage facilities based on real option model considering gas market reform in China. Energy Economics, 2018, 70, 132-142.	12.1	46
92	Three-dimensional geometric modeling of the cochlea using helico-spiral approximation. IEEE Transactions on Biomedical Engineering, 2000, 47, 1392-1402.	4.2	45
93	Machine learning will transform radiology significantly within the next 5 years. Medical Physics, 2017, 44, 2041-2044.	3.0	45
94	A tensor PRISM algorithm for multi-energy CT reconstruction and comparative studies. Journal of X-Ray Science and Technology, 2014, 22, 147-163.	1.0	43
95	Immunotherapy is associated with improved survival and decreased neurologic death after SRS for brain metastases from lung and melanoma primaries. Neuro-Oncology Practice, 2019, 6, 402-409.	1.6	43
96	Low-Dose CT Image Denoising Using a Generative Adversarial Network With a Hybrid Loss Function for Noise Learning. IEEE Access, 2020, 8, 67519-67529.	4.2	43
97	Deep learning predicts cardiovascular disease risks from lung cancer screening low dose computed tomography. Nature Communications, 2021, 12, 2963.	12.8	43
98	A parallel adaptive finite element simplified spherical harmonics approximation solver for frequency domain fluorescence molecular imaging. Physics in Medicine and Biology, 2010, 55, 4625-4645.	3.0	42
99	A dual-stream deep convolutional network for reducing metal streak artifacts in CT images. Physics in Medicine and Biology, 2019, 64, 235003.	3.0	41
100	Guest Editorial Compressive Sensing for Biomedical Imaging. IEEE Transactions on Medical Imaging, 2011, 30, 1013-1016.	8.9	40
101	Deep learning methods for CT image-domain metal artifact reduction. , 2017, , .		40
102	AirNet: Fused analytical and iterative reconstruction with deep neural network regularization for sparseâ€data CT. Medical Physics, 2020, 47, 2916-2930.	3.0	39
103	A backprojection-filtration algorithm for nonstandard spiral cone-beam CT with ann-Pl-window. Physics in Medicine and Biology, 2005, 50, 2099-2111.	3.0	38
104	Spectrally resolving and scattering-compensated x-ray luminescenceâ^fluorescence computed tomography. Journal of Biomedical Optics, 2011, 16, 066014.	2.6	38
105	Towards Omni-Tomography—Grand Fusion of Multiple Modalities for Simultaneous Interior Tomography. PLoS ONE, 2012, 7, e39700.	2.5	38
106	Temperature-modulated bioluminescence tomography. Optics Express, 2006, 14, 7852.	3.4	37
107	Deep learning methods to guide CT image reconstruction and reduce metal artifacts. Proceedings of SPIE, 2017, , .	0.8	37
108	Optimal pitch in spiral computed tomography. Medical Physics, 1997, 24, 1635-1639.	3.0	36

#	Article	IF	CITATIONS
109	A knowledge-based cone-beam x-ray CT algorithm for dynamic volumetric cardiac imaging. Medical Physics, 2002, 29, 1807-1822.	3.0	36
110	Cine Cardiac MRI Motion Artifact Reduction Using a Recurrent Neural Network. IEEE Transactions on Medical Imaging, 2021, 40, 2170-2181.	8.9	36
111	Exact BPF and FBP algorithms for nonstandard saddle curves. Medical Physics, 2005, 32, 3305-3312.	3.0	35
112	Design, analysis and simulation for development of the first clinical micro-CT scanner1. Academic Radiology, 2005, 12, 511-525.	2.5	35
113	Tomography-based 3-D anisotropic elastography using boundary measurements. IEEE Transactions on Medical Imaging, 2005, 24, 1323-1333.	8.9	35
114	A study on tetrahedron-based inhomogeneous Monte Carlo optical simulation. Biomedical Optics Express, 2011, 2, 44.	2.9	34
115	Study on the promotion of natural gas-fired electricity with energy market reform in China using a dynamic game-theoretic model. Applied Energy, 2017, 185, 1832-1839.	10.1	34
116	A General Total Variation Minimization Theorem for Compressed Sensing Based Interior Tomography. International Journal of Biomedical Imaging, 2009, 2009, 1-3.	3.9	33
117	SART-Type Image Reconstruction from a Limited Number of Projections with the Sparsity Constraint. International Journal of Biomedical Imaging, 2010, 2010, 1-9.	3.9	33
118	Analytic Comparison Between X-Ray Fluorescence CT and K-Edge CT. IEEE Transactions on Biomedical Engineering, 2014, 61, 975-985.	4.2	33
119	Super-resolution MRI and CT through GAN-CIRCLE. , 2019, , .		33
120	High-kVp Assisted Metal Artifact Reduction for X-Ray Computed Tomography. IEEE Access, 2016, 4, 4769-4776.	4.2	32
121	A new type of neurons for machine learning. International Journal for Numerical Methods in Biomedical Engineering, 2018, 34, e2920.	2.1	32
122	Visual Attention Network for Low-Dose CT. IEEE Signal Processing Letters, 2019, 26, 1152-1156.	3.6	32
123	The First Bioluminescence Tomography System for Simultaneous Acquisition of Multiview and Multispectral Data. International Journal of Biomedical Imaging, 2006, 2006, 1-8.	3.9	31
124	X-Optogenetics and U-Optogenetics: Feasibility and Possibilities. Photonics, 2015, 2, 23-39.	2.0	31
125	High-Resolution Mesoscopic Fluorescence Molecular Tomography Based on Compressive Sensing. IEEE Transactions on Biomedical Engineering, 2015, 62, 248-255.	4.2	31
126	Z-Index Parameterization for Volumetric CT Image Reconstruction via 3-D Dictionary Learning. IEEE Transactions on Medical Imaging, 2017, 36, 2466-2478.	8.9	31

#	Article	IF	CITATIONS
127	Feldkamp-type VOI reconstruction from super-short-scan cone-beam data. Medical Physics, 2004, 31, 1357-1362.	3.0	30
128	Combination of current-integrating/photon-counting detector modules for spectral CT. Physics in Medicine and Biology, 2013, 58, 7009-7024.	3.0	30
129	Parameter-Transferred Wasserstein Generative Adversarial Network (PT-WGAN) for Low-Dose PET Image Denoising. IEEE Transactions on Radiation and Plasma Medical Sciences, 2021, 5, 213-223.	3.7	30
130	Unwrapping cochlear implants by spiral CT. IEEE Transactions on Biomedical Engineering, 1996, 43, 891-900.	4.2	29
131	A Grangeat-type half-scan algorithm for cone-beam CT. Medical Physics, 2003, 30, 689-700.	3.0	29
132	An error-reduction-based algorithm for cone-beam computed tomography. Medical Physics, 2004, 31, 3206-3212.	3.0	29
133	Boundary integral method for bioluminescence tomography. Journal of Biomedical Optics, 2006, 11, 020503.	2.6	29
134	Vision 20/20: Simultaneous CTâ€MRI — Next chapter of multimodality imaging. Medical Physics, 2015, 42, 5879-5889.	3.0	29
135	Spectral CT Reconstruction—ASSIST: Aided by Self-Similarity in Image-Spectral Tensors. IEEE Transactions on Computational Imaging, 2019, 5, 420-436.	4.4	29
136	Local ROI Reconstruction via Generalized FBP and BPF Algorithms along More Flexible Curves. International Journal of Biomedical Imaging, 2006, 2006, 1-7.	3.9	28
137	Multisource X-Ray and CT: Lessons Learned and Future Outlook. IEEE Access, 2014, 2, 1568-1585.	4.2	28
138	Preliminary study on helical CT algorithms for patient motion estimation and compensation. IEEE Transactions on Medical Imaging, 1995, 14, 205-211.	8.9	27
139	An iterative algorithm for X-ray CT fluoroscopy. IEEE Transactions on Medical Imaging, 1998, 17, 853-856.	8.9	27
140	Threeâ€dimensional xâ€ray fluorescence mapping of a gold nanoparticleâ€loaded phantom. Medical Physics, 2014, 41, 031902.	3.0	27
141	Universal approximation with quadratic deep networks. Neural Networks, 2020, 124, 383-392.	5.9	27
142	Wavelet Sampling and Localization Schemes for the Radon Transform in Two Dimensions. SIAM Journal on Applied Mathematics, 1997, 57, 1749-1762.	1.8	26
143	Three-dimensional modeling and visualization of the cochlea on the Internet. IEEE Transactions on Information Technology in Biomedicine, 2000, 4, 144-151.	3.2	26
144	Feldkamp-type cone-beam tomography in the wavelet framework. IEEE Transactions on Medical Imaging, 2000, 19, 922-929.	8.9	26

#	Article	IF	CITATIONS
145	Minimum detection windows, PI-line existence and uniqueness for helical cone-beam scanning of variable pitch. Medical Physics, 2004, 31, 566-572.	3.0	26
146	An intuitive discussion on the ideal ramp filter in computed tomography (I). Computers and Mathematics With Applications, 2005, 49, 731-740.	2.7	26
147	Differential phase-contrast interior tomography. Physics in Medicine and Biology, 2012, 57, 2905-2914.	3.0	26
148	Virtual Monoenergetic CT Imaging via Deep Learning. Patterns, 2020, 1, 100128.	5.9	26
149	Deep Efficient End-to-End Reconstruction (DEER) Network for Few-View Breast CT Image Reconstruction. IEEE Access, 2020, 8, 196633-196646.	4.2	26
150	Straightening the colon with curved cross sections: An approach to CT colonography. Academic Radiology, 1999, 6, 398-410.	2.5	25
151	Differential Evolution Approach for Regularized Bioluminescence Tomography. IEEE Transactions on Biomedical Engineering, 2010, 57, 2229-2238.	4.2	25
152	Low-dose CT via deep CNN with skip connection and network-in-network. , 2019, , .		25
153	Spatial Variation of Resolution and Noise in Multi–Detector Row Spiral CT. Academic Radiology, 2003, 10, 607-613.	2.5	24
154	Image reconstruction from limited angle projections collected by multisource interior x-ray imaging systems. Physics in Medicine and Biology, 2011, 56, 6337-6357.	3.0	24
155	CAM-CM: a signal deconvolution tool for <i>in vivo</i> dynamic contrast-enhanced imaging of complex tissues. Bioinformatics, 2011, 27, 2607-2609.	4.1	24
156	Hybrid Spectral Micro-CT: System Design, Implementation, and Preliminary Results. IEEE Transactions on Biomedical Engineering, 2014, 61, 246-253.	4.2	24
157	Energy Window Optimization for X-Ray K-Edge Tomographic Imaging. IEEE Transactions on Biomedical Engineering, 2016, 63, 1623-1630.	4.2	24
158	Corrective regulations on renewable energy certificates trading: Pursuing an equity-efficiency trade-off. Energy Economics, 2019, 80, 970-982.	12.1	24
159	Synergizing medical imaging and radiotherapy with deep learning. Machine Learning: Science and Technology, 2020, 1, 021001.	5.0	24
160	Fractional scan algorithms for low-dose perfusion CT. Medical Physics, 2004, 31, 1254-1257.	3.0	23
161	A differentiable Shepp–Logan phantom and its applications in exact cone-beam CT. Physics in Medicine and Biology, 2005, 50, 5583-5595.	3.0	23
162	A Fast CT Reconstruction Scheme for a General Multi-Core PC. International Journal of Biomedical Imaging, 2007, 2007, 1-9.	3.9	23

#	Article	IF	CITATIONS
163	A Filtered Backprojection Algorithm for Triple-Source Helical Cone-Beam CT. IEEE Transactions on Medical Imaging, 2009, 28, 384-393.	8.9	23
164	Compressive Sensing–Based Interior Tomography. Journal of Computer Assisted Tomography, 2011, 35, 762-764.	0.9	23
165	High-order total variation minimization for interior SPECT. Inverse Problems, 2012, 28, 015001.	2.0	23
166	Scout-view assisted interior micro-CT. Physics in Medicine and Biology, 2013, 58, 4297-4314.	3.0	23
167	A novel calibration method incorporating nonlinear optimization and ballâ€bearing markers for coneâ€beam CT with a parameterized trajectory. Medical Physics, 2019, 46, 152-164.	3.0	23
168	Accelerated Correction of Reflection Artifacts by Deep Neural Networks in Photo-Acoustic Tomography. Applied Sciences (Switzerland), 2019, 9, 2615.	2.5	23
169	Knowledge-Based Analysis for Mortality Prediction From CT Images. IEEE Journal of Biomedical and Health Informatics, 2020, 24, 457-464.	6.3	23
170	Formulation of photon diffusion from spherical bioluminescent sources in an infinite homogeneous medium. BioMedical Engineering OnLine, 2004, 3, 12.	2.7	22
171	Completeness map evaluation demonstrated with candidate nextâ€generation cardiac CT architectures. Medical Physics, 2012, 39, 2405-2416.	3.0	22
172	A bibliometric analysis of academic publication and NIH funding. Journal of Informetrics, 2013, 7, 318-324.	2.9	22
173	X-ray micromodulated luminescence tomography in dual-cone geometry. Journal of Biomedical Optics, 2014, 19, 076002.	2.6	22
174	Theoretical and numerical analysis on multispectral bioluminescence tomography. IMA Journal of Applied Mathematics, 2007, 72, 67-85.	1.6	21
175	Morphometric differences between central vs. surface acini in A/J mice using high-resolution micro-computed tomography. Journal of Applied Physiology, 2016, 121, 115-122.	2.5	21
176	Simultaneous CT-MRI Reconstruction for Constrained Imaging Geometries Using Structural Coupling and Compressive Sensing. IEEE Transactions on Biomedical Engineering, 2016, 63, 1301-1309.	4.2	21
177	Deep Encoder-Decoder Adversarial Reconstruction (DEAR) Network for 3D CT from Few-View Data. Bioengineering, 2019, 6, 111.	3.5	21
178	Low-contrast resolution in volumetric x-ray CT-Analytical comparison between conventional and spiral CT. Medical Physics, 1997, 24, 373-376.	3.0	20
179	PI-line-based image reconstruction in helical cone-beam computed tomography with a variable pitch. Medical Physics, 2005, 32, 2639-2648.	3.0	20
180	Analysis on the strip-based projection model for discrete tomography. Discrete Applied Mathematics, 2008, 156, 2359-2367.	0.9	20

#	Article	IF	CITATIONS
181	X-Ray Phase-Contrast Imaging with Three 2D Gratings. International Journal of Biomedical Imaging, 2008, 2008, 1-8.	3.9	20
182	X-ray fluorescence tomographic system design and image reconstruction. Journal of X-Ray Science and Technology, 2013, 21, 1-8.	1.0	20
183	Dynamic Bowtie Filter for Cone-Beam/Multi-Slice CT. PLoS ONE, 2014, 9, e103054.	2.5	20
184	Edge-Guided Dual-Modality Image Reconstruction. IEEE Access, 2014, 2, 1359-1363.	4.2	20
185	Multi-region optimal deployment of renewable energy considering different interregional transmission scenarios. Energy, 2016, 108, 108-118.	8.8	20
186	Computed tomography simulation with superquadrics. Medical Physics, 2005, 32, 3136-3143.	3.0	19
187	Interior SPECT—exact and stable ROI reconstruction from uniformly attenuated local projections. Communications in Numerical Methods in Engineering, 2009, 25, 693-710.	1.3	19
188	Three-Dimensional Characterization of Iron Oxide (α-Fe ₂ O ₃) Nanoparticles: Application of a Compressed Sensing Inspired Reconstruction Algorithm to Electron Tomography. Microscopy and Microanalysis, 2012, 18, 1362-1367.	0.4	19
189	Possible Animal Embryos from the Lower Cambrian (Stage 3) Shuijingtuo Formation, Hubei Province, South China. Journal of Paleontology, 2014, 88, 385-394.	0.8	19
190	Geometric studies on variable radius spiral cone-beam scanning. Medical Physics, 2004, 31, 1473-1480.	3.0	18
191	Interior Tomography With Continuous Singular Value Decomposition. IEEE Transactions on Medical Imaging, 2012, 31, 2108-2119.	8.9	18
192	Fast and accurate computation of system matrix for area integral model-based algebraic reconstruction technique. Optical Engineering, 2014, 53, 113101.	1.0	18
193	X-ray CT geometrical calibration via locally linear embedding. Journal of X-Ray Science and Technology, 2016, 24, 241-256.	1.0	18
194	MCDNet – A Denoising Convolutional Neural Network to Accelerate Monte Carlo Radiation Transport Simulations: A Proof of Principle With Patient Dose From X-Ray CT Imaging. IEEE Access, 2019, 7, 76680-76689.	4.2	18
195	Experimental studies on few-view reconstruction for high-resolution micro-CT. Journal of X-Ray Science and Technology, 2013, 21, 25-42.	1.0	17
196	Interior microâ \in CT with an offset detector. Medical Physics, 2014, 41, 061915.	3.0	17
197	Generalized backpropagation algorithm for training secondâ€order neural networks. International Journal for Numerical Methods in Biomedical Engineering, 2018, 34, e2956.	2.1	17
198	Learning From Pseudo-Randomness With an Artificial Neural Network–Does God Play Pseudo-Dice?. IEEE Access, 2018, 6, 22987-22992.	4.2	17

#	Article	IF	CITATIONS
199	Automatic measurement of the labyrinth using image registration and a deformable inner ear atlas. Academic Radiology, 2003, 10, 988-999.	2.5	16
200	Cone-beam pseudo-lambda tomography. Inverse Problems, 2007, 23, 203-215.	2.0	16
201	A Fiber-Optic-Based Imaging System for Nondestructive Assessment of Cell-Seeded Tissue-Engineered Scaffolds. Tissue Engineering - Part C: Methods, 2012, 18, 677-687.	2.1	16
202	A twoâ€dimensional feasibility study of deep learningâ€based feature detection and characterization directly from CT sinograms. Medical Physics, 2019, 46, e790-e800.	3.0	16
203	Optical tomographic imaging for breast cancer detection. Journal of Biomedical Optics, 2017, 22, 1.	2.6	16
204	Temporal bone volumetric image deblurring in spiral computed tomography scanning. Academic Radiology, 1995, 2, 888-895.	2.5	15
205	Maximum volume coverage in spiral computed tomography scanning. Academic Radiology, 1996, 3, 423-428.	2.5	15
206	Axiomatic approach for quantification of image resolution. IEEE Signal Processing Letters, 1999, 6, 257-258.	3.6	15
207	Blind deblurring of spiral CT images-comparative studies on edge-to-noise ratios. Medical Physics, 2002, 29, 821-829.	3.0	15
208	Evolution-Operator-Based Single-Step Method for Image Processing. International Journal of Biomedical Imaging, 2006, 2006, 1-27.	3.9	15
209	Mathematical Study and Numerical Simulation of Multispectral Bioluminescence Tomography. International Journal of Biomedical Imaging, 2006, 2006, 1-10.	3.9	15
210	Dynamic bowtie for fan-beam CT. Journal of X-Ray Science and Technology, 2013, 21, 579-590.	1.0	15
211	Convex Hull Aided Registration Method (CHARM). IEEE Transactions on Visualization and Computer Graphics, 2017, 23, 2042-2055.	4.4	15
212	Radiomics in lung cancer: Its time is here. Medical Physics, 2018, 45, 997-1000.	3.0	15
213	Unsupervised Deconvolution of Dynamic Imaging Reveals Intratumor Vascular Heterogeneity and Repopulation Dynamics. PLoS ONE, 2014, 9, e112143.	2.5	15
214	Practical cone-beam lambda tomography. Medical Physics, 2006, 33, 3640-3646.	3.0	14
215	Review of Parallel Computing Techniques for Computed Tomography Image Reconstruction. Current Medical Imaging, 2006, 2, 405-414.	0.8	14
216	Xâ€ray scatter correction for multiâ€source interior computed tomography. Medical Physics, 2017, 44, 71-83.	3.0	14

#	Article	IF	CITATIONS
217	Artifacts associated with implementation of the Grangeat formula. Medical Physics, 2002, 29, 2871-2880.	3.0	13
218	A general exact method for synthesizing parallel-beam projections from cone-beam projections via filtered backprojection. Physics in Medicine and Biology, 2006, 51, 5643-5654.	3.0	13
219	A Theoretical Framework of X-Ray Dark-Field Tomography. SIAM Journal on Applied Mathematics, 2011, 71, 1557-1577.	1.8	13
220	Scanning-fiber-based imaging method for tissue engineering. Journal of Biomedical Optics, 2012, 17, 066010.	2.6	13
221	Market Analysis of Natural Gas for District Heating in China. Energy Procedia, 2015, 75, 2713-2717.	1.8	13
222	Fuzzy logic interpretation of quadratic networks. Neurocomputing, 2020, 374, 10-21.	5.9	13
223	Attention augmented multi-scale network for single image super-resolution. Applied Intelligence, 2021, 51, 935-951.	5.3	13
224	Fast algorithm for soft straightening of the colon. Academic Radiology, 2000, 7, 142-148.	2.5	12
225	Anisotropic Elastography for Local Passive Properties and Active Contractility of Myocardium from Dynamic Heart Imaging Sequence. International Journal of Biomedical Imaging, 2006, 2006, 1-15.	3.9	12
226	Digital spectral separation methods and systems for bioluminescence imaging. Optics Express, 2008, 16, 1719.	3.4	12
227	Can interior tomography outperform lambda tomography?. Proceedings of the National Academy of Sciences of the United States of America, 2010, 107, E92-3, author reply E94-5.	7.1	12
228	Energy-discriminative performance of a spectral micro-CT system. Journal of X-Ray Science and Technology, 2013, 21, 335-345.	1.0	12
229	A Stationary-Sources and Rotating-Detectors Computed Tomography Architecture for Higher Temporal Resolution and Lower Radiation Dose. IEEE Access, 2014, 2, 1263-1271.	4.2	12
230	Pseudo progression identification of glioblastoma with dictionary learning. Computers in Biology and Medicine, 2016, 73, 94-101.	7.0	12
231	Hybrid Imaging System for Simultaneous Spiral MR and X-ray (MRX) Scans. IEEE Access, 2017, 5, 1050-1061.	4.2	12
232	Comparison of deep learning and human observer performance for detection and characterization of simulated lesions. Journal of Medical Imaging, 2019, 6, 1.	1.5	12
233	Deep Tomographic Image Reconstruction: Yesterday, Today, and Tomorrow—Editorial for the 2nd Special Issue "Machine Learning for Image Reconstruction― IEEE Transactions on Medical Imaging, 2021, 40, 2956-2964.	8.9	12
234	Reduction of Half-Scan Shading Artifact Based on Full-Scan Correction1. Academic Radiology, 2006, 13, 55-62.	2.5	11

#	Article	IF	CITATIONS
235	An Adaptive Optimal Control Design for a Bolus Chasing Computed Tomography Angiography. IEEE Transactions on Control Systems Technology, 2008, 16, 60-69.	5.2	11
236	Integral equations of the photon fluence rate and flux based on a generalized Delta-Eddington phase function. Journal of Biomedical Optics, 2008, 13, 024016.	2.6	11
237	Bioluminescence tomography with Gaussian prior. Biomedical Optics Express, 2010, 1, 1259.	2.9	11
238	On a family of differential approximations of the radiative transfer equation. Journal of Mathematical Chemistry, 2012, 50, 689-702.	1.5	11
239	Imaging and characterization of bioengineered blood vessels within a bioreactor using freeâ€space and catheterâ€based OCT. Lasers in Surgery and Medicine, 2013, 45, 391-400.	2.1	11
240	Design optimization of a periodic microstructured array anode for hard x-ray grating interferometry. Physics in Medicine and Biology, 2019, 64, 145011.	3.0	11
241	Impact of brain metastasis velocity on neurologic death for brain metastasis patients experiencing distant brain failure after initial stereotactic radiosurgery. Journal of Neuro-Oncology, 2020, 146, 285-292.	2.9	11
242	Soft Autoencoder and Its Wavelet Adaptation Interpretation. IEEE Transactions on Computational Imaging, 2020, 6, 1245-1257.	4.4	11
243	Simultaneous reconstruction of the initial pressure and sound speed in photoacoustic tomography using a deep-learning approach. , 2019, , .		11
244	CT image reconstruction on a low dimensional manifold. Inverse Problems and Imaging, 2019, 13, 449-460.	1.1	11
245	A localization algorithm and error analysis for stereo x-ray image guidance. Medical Physics, 2000, 27, 885-893.	3.0	10
246	Relation between the filtered backprojection algorithm and the backprojection algorithm in CT. IEEE Signal Processing Letters, 2005, 12, 633-636.	3.6	10
247	A General Formula for Fan-Beam Lambda Tomography. International Journal of Biomedical Imaging, 2006, 2006, 1-9.	3.9	10
248	A General Formula for Fan-Beam Lambda Tomography (Erratum). International Journal of Biomedical Imaging, 2007, 2007, 1-1.	3.9	10
249	Theoretical study on high order interior tomography. Journal of X-Ray Science and Technology, 2012, 20, 423-436.	1.0	10
250	Stored luminescence computed tomography. Applied Optics, 2014, 53, 5672.	1.8	10
251	An edge-on charge-transfer design for energy-resolved x-ray detection. Physics in Medicine and Biology, 2016, 61, 4183-4200.	3.0	10
252	Quest for the ultimate cardiac CT scanner. Medical Physics, 2017, 44, 4506-4524.	3.0	10

#	Article	IF	CITATIONS
253	Multifactorial Analysis of Mortality in Screening Detected Lung Cancer. Journal of Oncology, 2018, 2018, 1-7.	1.3	10
254	Deep learning for high-resolution and high-sensitivity interferometric phase contrast imaging. Scientific Reports, 2020, 10, 9891.	3.3	10
255	Dynamic, Nondestructive Imaging of a Bioengineered Vascular Graft Endothelium. PLoS ONE, 2013, 8, e61275.	2.5	10
256	Geometrical modeling using multiregional marching tetrahedra for bioluminescence tomography. , 2005, , .		9
257	Cone-beam mammo-computed tomography from data along two tilting arcs. Medical Physics, 2006, 33, 3621-3633.	3.0	9
258	Computational methods for optical molecular imaging. Communications in Numerical Methods in Engineering, 2009, 25, 1137-1161.	1.3	9
259	Gel'fand-Graev's reconstruction formula in the 3D real space. Medical Physics, 2011, 38, S69-S75.	3.0	9
260	X-ray micro-modulated luminescence tomography (XMLT). Optics Express, 2014, 22, 5572.	3.4	9
261	Talbot interferometry with curved quasi-periodic gratings: towards large field of view X-ray phase-contrast imaging. Optics Express, 2015, 23, 26576.	3.4	9
262	Nanophosphor-Based Contrast Agents for Spectral X-ray Imaging. Nanomaterials, 2019, 9, 1092.	4.1	9
263	Small-angle scatter tomography with a photon-counting detector array. Physics in Medicine and Biology, 2016, 61, 3734-3748.	3.0	9
264	Dual network architecture for few-view CT - trained on ImageNet data and transferred for medical imaging. , 2019, , .		9
265	Axiomatic quantification of multidimensional image resolution. IEEE Signal Processing Letters, 2002, 9, 120-122.	3.6	8
266	Axiomatic characterization of nonlinear homomorphic means. Journal of Mathematical Analysis and Applications, 2005, 303, 350-363.	1.0	8
267	General Formula for Fan-Beam Computed Tomography. Physical Review Letters, 2005, 95, 258102.	7.8	8
268	Bolus characteristics based on Magnetic Resonance Angiography. BioMedical Engineering OnLine, 2006, 5, 53.	2.7	8
269	Lambda tomography with discontinuous scanning trajectories. Physics in Medicine and Biology, 2007, 52, 4331-4344.	3.0	8
270	PARAMETRIC STUDY OF TISSUE OPTICAL CLEARING BY LOCALIZED MECHANICAL COMPRESSION USING COMBINED FINITE ELEMENT AND MONTE CARLO SIMULATION. Journal of Innovative Optical Health Sciences, 2010, 03, 203-211.	1.0	8

#	Article	IF	CITATIONS
271	Higher-order phase shift reconstruction approach. Medical Physics, 2010, 37, 5238-5242.	3.0	8
272	X-Ray Fluorescence Computed Tomography With Polycapillary Focusing. IEEE Access, 2014, 2, 1138-1142.	4.2	8
273	Top-level design and pilot analysis of low-end CT scanners based on linear scanning for developing countries. Journal of X-Ray Science and Technology, 2014, 22, 673-686.	1.0	8
274	Dictionaryâ€learningâ€based reconstruction method for electron tomography. Scanning, 2014, 36, 377-383.	1.5	8
275	Guest Editorial Special Issue on Spectral CT. IEEE Transactions on Medical Imaging, 2015, 34, 693-696.	8.9	8
276	Study on the Implementation Pathways and Key Impacts of RPS Target in China using a Dynamic Game-Theoretical Equilibrium Power Market Model. Energy Procedia, 2017, 105, 3844-3849.	1.8	8
277	Model and reconstruction of a K-edge contrast agent distribution with an X-ray photon-counting detector. Optics Express, 2017, 25, 9378.	3.4	8
278	Increased separability of K-edge nanoparticles by photon-counting detectors for spectral micro-CT. Journal of X-Ray Science and Technology, 2018, 26, 707-726.	1.0	8
279	Conception and policy implications of photovoltaic modules endâ€ofâ€life management in China. Wiley Interdisciplinary Reviews: Energy and Environment, 2021, 10, .	4.1	8
280	Spectral X-Ray CT Image Reconstruction with a Combination of Energy-Integrating and Photon-Counting Detectors. PLoS ONE, 2016, 11, e0155374.	2.5	8
281	A novel transfer learning framework for low-dose CT. , 2019, , .		8
282	An ensemble learning method based on ordinal regression for COVID-19 diagnosis from chest CT. Physics in Medicine and Biology, 2021, 66, 244001.	3.0	8
283	Localization of cochlear implant electrodes in radiographs. Medical Physics, 2000, 27, 775-777.	3.0	7
284	Adaptive bolus chasing computed tomography angiography: Control scheme and experimental results. Biomedical Signal Processing and Control, 2008, 3, 319-326.	5.7	7
285	Demonstration of Dose and Scatter Reductions for Interior Computed Tomography. Journal of Computer Assisted Tomography, 2009, 33, 967-972.	0.9	7
286	A novel approach for studies of multispectral bioluminescence tomography. Numerische Mathematik, 2010, 115, 553-583.	1.9	7
287	Fast Exact/Quasi-Exact FBP Algorithms for Triple-Source Helical Cone-Beam CT. IEEE Transactions on Medical Imaging, 2010, 29, 756-770.	8.9	7
288	Compressed Sensing Inspired Image Reconstruction from Overlapped Projections. International Journal of Biomedical Imaging, 2010, 2010, 1-8.	3.9	7

#	Article	IF	CITATIONS
289	SART-Type Image Reconstruction from Overlapped Projections. International Journal of Biomedical Imaging, 2011, 2011, 1-7.	3.9	7
290	TV-Based image reconstruction of multiple objects in a fixed source-detector geometry. Journal of X-Ray Science and Technology, 2012, 20, 277-289.	1.0	7
291	Spherical grating based xâ€ray Talbot interferometry. Medical Physics, 2015, 42, 6514-6519.	3.0	7
292	A skeleton-tree-based approach to acinar morphometric analysis using microcomputed tomography with comparison of acini in young and old C57BL/6 mice. Journal of Applied Physiology, 2016, 120, 1402-1409.	2.5	7
293	Correction for "3D Convolutional Encoder-Decoder Network for Low-Dose CT via Transfer Learning From a 2D Trained Network―[Jun 18 1522-1534]. IEEE Transactions on Medical Imaging, 2018, 37, 2750-2750.	8.9	7
294	A new iterative algorithm for ring artifact reduction in CT using ring total variation. Medical Physics, 2019, 46, 4803-4815.	3.0	7
295	Focused x-ray luminescence imaging system for small animals based on a rotary gantry. Journal of Biomedical Optics, 2021, 26, .	2.6	7
296	General rigid motion correction for computed tomography imaging based on locally linear embedding. Optical Engineering, 2018, 57, 1.	1.0	7
297	Clinical Micro-CT Empowered by Interior Tomography, Robotic Scanning, and Deep Learning. IEEE Access, 2020, 8, 229018-229032.	4.2	7
298	Computational optical biopsy. BioMedical Engineering OnLine, 2005, 4, 36.	2.7	6
299	Cone-Beam Composite-Circling Scan and Exact Image Reconstruction for a Quasi-Short Object. International Journal of Biomedical Imaging, 2007, 2007, 1-10.	3.9	6
300	Digital Eversion of a Hollow Structure: An Application in Virtual Colonography. International Journal of Biomedical Imaging, 2008, 2008, 1-6.	3.9	6
301	Parallelism of iterative CT reconstruction based onÂlocal reconstruction algorithm. Journal of Supercomputing, 2009, 48, 1-14.	3.6	6
302	Fourier transform-based iterative method for differential phase-contrast computed tomography. Optics Letters, 2012, 37, 1784.	3.3	6
303	Dictionary Learning Based Low-Dose X-Ray CT Reconstruction. , 2014, , 99-119.		6
304	Dictionary learning based low-dose x-ray CT reconstruction using a balancing principle. , 2014, , .		6
305	Dynamic Assessment of the Endothelialization of Tissue-Engineered Blood Vessels Using an Optical Coherence Tomography Catheter-Based Fluorescence Imaging System. Tissue Engineering - Part C: Methods, 2015, 21, 758-766.	2.1	6
306	The impact of social network on the adoption of real-time electricity pricing mechanism. Energy Procedia, 2017, 142, 3154-3159.	1.8	6

#	Article	IF	CITATIONS
307	Techniques of CT Colonography (Virtual Colonoscopy). Critical Reviews in Biomedical Engineering, 1999, 27, 1-25.	0.9	6
308	Modeling of moral decisions with deep learning. Visual Computing for Industry, Biomedicine, and Art, 2020, 3, 27.	3.7	6
309	Digital X-ray stereophotogrammetry for cochlear implantation. IEEE Transactions on Biomedical Engineering, 2000, 47, 1120-1130.	4.2	5
310	Design of a dual CCD configuration to improve the signal-to-noise ratio. Medical Physics, 2000, 27, 2435-2437.	3.0	5
311	Localization error analysis for stereo X-ray image guidance with probability method. Medical Engineering and Physics, 2001, 23, 573-581.	1.7	5
312	Three-Dimensional Localization of Cochlear Implant Electrodes Using Epipolar Stereophotogrammetry. IEEE Transactions on Biomedical Engineering, 2004, 51, 838-846.	4.2	5
313	MicroCT-guided Bioluminescence Tomography Based on the Adaptive Finite Element Tomographic Algorithm. , 2006, 2006, 381-4.		5
314	Studies on Palamodov's algorithm for cone-beam CT along a general curve. Inverse Problems, 2006, 22, 447-460.	2.0	5
315	Digital Tomosynthesis Aided by Low-Resolution Exact Computed Tomography. Journal of Computer Assisted Tomography, 2007, 31, 976-983.	0.9	5
316	A comparative study on interpolation methods for controlled cardiac CT. International Journal of Imaging Systems and Technology, 2007, 17, 91-98.	4.1	5
317	An integrated solution and analysis of bioluminescence tomography and diffuse optical tomography. Communications in Numerical Methods in Engineering, 2009, 25, 639-656.	1.3	5
318	Exact image reconstruction with triple-source saddle-curve cone-beam scanning. Physics in Medicine and Biology, 2009, 54, 2971-2991.	3.0	5
319	Monte Carlo fluorescence microtomography. Journal of Biomedical Optics, 2011, 16, 070501.	2.6	5
320	Upper-Bound on Dose Reduction in CT Reconstruction for Nodule Detection. IEEE Access, 2016, 4, 4247-4253.	4.2	5
321	Cardiac CT: A system architecture study. Journal of X-Ray Science and Technology, 2016, 24, 43-65.	1.0	5
322	Fluorescent imaging of endothelial cells in bioengineered blood vessels: the impact of crosslinking of the scaffold. Journal of Tissue Engineering and Regenerative Medicine, 2016, 10, 955-966.	2.7	5
323	Grating Oriented Line-Wise Filtration (GOLF) for Dual-Energy X-ray CT. Sensing and Imaging, 2017, 18, 1.	1.5	5

324 Quadratic autoencoder for low-dose CT denoising. , 2019, , .

#	Article	IF	CITATIONS
325	Radiologic volumetry on a personal computer with a stereologic method. Academic Radiology, 1998, 5, 665-669.	2.5	4
326	Distortion reduction for fast soft straightening of the colon. Academic Radiology, 2000, 7, 506-515.	2.5	4
327	Controlled Cardiac Computed Tomography. International Journal of Biomedical Imaging, 2006, 2006, 1-11.	3.9	4
328	Recent Development in Bioluminescence Tomography. , 0, , .		4
329	Line-Source Based X-Ray Tomography. International Journal of Biomedical Imaging, 2009, 2009, 1-8.	3.9	4
330	Temperature-Change-Based Thermal Tomography. International Journal of Biomedical Imaging, 2009, 2009, 1-4.	3.9	4
331	Top-Level System Designs for Hybrid Low-Field MRI–CT with Potential of Pulmonary Imaging. Sensing and Imaging, 2014, 15, 1.	1.5	4
332	Image reconstruction for x-ray K-edge imaging with a photon counting detector. , 2014, , .		4
333	Data consistency condition for truncated projections in fan-beam geometry. Journal of X-Ray Science and Technology, 2015, 23, 627-638.	1.0	4
334	A framelet-based iterative maximum-likelihood reconstruction algorithm for spectral CT. Inverse Problems, 2016, 32, 115021.	2.0	4
335	High-resolution X-ray phase-contrast imaging with a grating interferometer. Journal of the Korean Physical Society, 2017, 71, 538-542.	0.7	4
336	Study of the impacts of upstream natural gas market reform in China on infrastructure deployment and social welfare using an SVM-based rolling horizon stochastic game analysis. Petroleum Science, 2018, 15, 898-911.	4.9	4
337	Novel Detection Scheme for X-Ray Small-Angle Scattering. IEEE Transactions on Radiation and Plasma Medical Sciences, 2018, 2, 315-325.	3.7	4
338	A novel framework for the NMF methods with experiments to unmixing signals and feature representation. Journal of Computational and Applied Mathematics, 2019, 362, 205-218.	2.0	4
339	A Reconfigurable energy-resolving method for a layered edge-on detector. Physics in Medicine and Biology, 2019, 64, 135008.	3.0	4
340	Modeling and Policy Study for Information Asymmetry Problem of Photovoltaic Module Quality in China. Emerging Markets Finance and Trade, 2021, 57, 653-667.	3.1	4
341	A directional TV based ring artifact reduction method. , 2019, , .		4
342	Deep-learning-based breast CT for radiation dose reduction. , 2019, , .		4

Deep-learning-based breast CT for radiation dose reduction. , 2019, , . 342

#	Article	IF	CITATIONS
343	Multi-task learning for mortality prediction in LDCT images. , 2020, , .		4
344	Quadratic neural networks for CT metal artifact reduction. , 2019, , .		4
345	Wavelet filtering algorithm for fan-beam CT. Electronics Letters, 1998, 34, 2395.	1.0	3
346	Experimental System for X-ray Cone-Beam Microtomography. Microscopy and Microanalysis, 1998, 4, 56-62.	0.4	3
347	Interpolation algorithms for digital mammography systems with multiple detectors. Academic Radiology, 1999, 6, 170-175.	2.5	3
348	Minimum detection window and inter-helix PI-line with triple-source helical cone-beam scanning. , 2004, , .		3
349	A general scheme for velocity tomography. Signal Processing, 2008, 88, 1165-1175.	3.7	3
350	Knowledge-Based Dynamic Volumetric Cardiac Computed Tomography With Saddle Curve Trajectory. Journal of Computer Assisted Tomography, 2008, 32, 942-950.	0.9	3
351	In Situ Real-Time Chemiluminescence Imaging of Reactive Oxygen Species Formation from Cardiomyocytes. International Journal of Biomedical Imaging, 2008, 2008, 1-9.	3.9	3
352	Piecewise-Constant-Model-Based Interior Tomography Applied to Dentin Tubules. Computational and Mathematical Methods in Medicine, 2013, 2013, 1-8.	1.3	3
353	X-ray fan-beam luminescence tomography. , 2014, , .		3
354	Spectral CT reconstruction using image sparsity and spectral correlation. , 2015, , .		3
355	Market Analysis of Natural Gas for Power Generation in China. Energy Procedia, 2015, 75, 2718-2723.	1.8	3
356	Fully 3D geometrical calibration forÂanÂX-ray grating-based imaging system. Journal of X-Ray Science and Technology, 2016, 24, 821-836.	1.0	3
357	A spectral interior CT by a framelet-based reconstruction algorithm. Journal of X-Ray Science and Technology, 2016, 24, 771-785.	1.0	3
358	Edge-oriented dual-dictionary guided enrichment (EDGE) for MRI-CT image reconstruction. Journal of X-Ray Science and Technology, 2016, 24, 161-175.	1.0	3
359	Radiative transfer with delta-Eddington-type phase functions. Applied Mathematics and Computation, 2017, 300, 70-78.	2.2	3
360	E-Index—A Bibliometric Index of Research Efficiency. IEEE Access, 2018, 6, 51355-51364.	4.2	3

#	Article	IF	CITATIONS
361	Monochromatic image reconstruction via machine learning. Machine Learning: Science and Technology, 2021, 2, 025032.	5.0	3
362	Metal artifact reduction for radiation therapy: a simulation study. , 2018, , .		3
363	Non-uniformity correction for MARS photon-counting detectors. , 2019, , .		3
364	X-ray luminescence imaging for small animals. , 2020, 11224, .		3
365	Selectable Source Rotational Velocity for Cardiac Computed Tomography. Journal of Computer Assisted Tomography, 2007, 31, 16-21.	0.9	2
366	Studies of a mathematical model for temperature-modulated bioluminescence tomography. Applicable Analysis, 2009, 88, 193-213.	1.3	2
367	Adaptive bolus-chasing computed tomography angiography in the cases of symmetric and asymmetric ard arteric ard arterial flows in peripheral arteries. Biomedical Signal Processing and Control, 2009, 4, 302-308.	5.7	2
368	SLATE: Virtualizing multiscale CT training. Journal of X-Ray Science and Technology, 2012, 20, 239-248.	1.0	2
369	A self-adaptive mask-enhanced dual-dictionary learning method for MRI-CT image reconstruction. , 2015, , .		2
370	Combined Impacts of RTP and FIT on Optimal Management for a Residential Micro-Grid. Energy Procedia, 2015, 75, 1666-1672.	1.8	2
371	A mixed reality approach for stereo-tomographic quantification of lung nodules. Journal of X-Ray Science and Technology, 2016, 24, 615-625.	1.0	2
372	Study on the Impacts of the LNG Market Reform in China using a SVM based Rolling Horizon Stochastic Game Analysis. Energy Procedia, 2017, 105, 3850-3855.	1.8	2
373	Simultaneous Emission-Transmission Tomography in an MRI Hardware Framework. IEEE Transactions on Radiation and Plasma Medical Sciences, 2018, 2, 326-336.	3.7	2
374	Wavelet-based joint CT-MRI reconstruction. Journal of X-Ray Science and Technology, 2018, 26, 379-393.	1.0	2
375	Sound Transmission-Based Elastography Imaging. IEEE Access, 2019, 7, 74383-74392.	4.2	2
376	Hybrid Neural Networks for Mortality Prediction from LDCT Images. , 2019, 2019, 6243-6246.		2
377	A framework for least squares nonnegative matrix factorizations with Tikhonov regularization. Neurocomputing, 2020, 387, 78-90.	5.9	2
378	Compton-camera-based SPECT for thyroid cancer imaging. Journal of X-Ray Science and Technology, 2021, 29, 111-124.	1.0	2

#	Article	IF	CITATIONS
379	Modulated luminescence tomography. Inverse Problems and Imaging, 2015, 9, 579-589.	1.1	2
380	Generative Low-Dose CT Image Denoising. Advances in Computer Vision and Pattern Recognition, 2019, , 277-297.	1.3	2
381	Comparison of deep learning and human observer performance for lesion detection and characterization. , 2019, , .		2
382	Low-dose CT simulation with a generative adversarial network. , 2019, , .		2
383	Phase function estimation from a diffuse optical image via deep learning. Physics in Medicine and Biology, 2022, 67, 074001.	3.0	2
384	Adaptive image interpolation for full-field digital x-ray mammography. Applied Optics, 1999, 38, 253.	2.1	1
385	A general axiomatic system for image resolution quantification. Journal of Mathematical Analysis and Applications, 2006, 315, 462-473.	1.0	1
386	Message from the Editor-in-Chief. International Journal of Biomedical Imaging, 2006, 2006, 1-2.	3.9	1
387	Determination of exact reconstruction regions in composite-circling cone-beam tomography. Medical Physics, 2009, 36, 3448-3454.	3.0	1
388	Varying Collimation for Dark-Field Extraction. International Journal of Biomedical Imaging, 2009, 2009, 2009, 1-7.	3.9	1
389	On a Derivative-Free Fan-Beam Reconstruction Formula. IEEE Transactions on Image Processing, 2011, 20, 1173-1176.	9.8	1
390	Tetrahedron-based orthogonal simultaneous scan for cone-beam computed tomography. Optical Engineering, 2012, 51, 1.	1.0	1
391	Carotid plaque characterization using CT and MRI scans for synergistic image analysis. , 2014, , .		1
392	Study of scan protocol for exposure reduction in hybrid spectral micro T. Scanning, 2014, 36, 444-455.	1.5	1
393	Comparison of lp-regularization-based reconstruction methods for time domain fluorescence molecular tomography on early time gates. , 2014, , .		1
394	Rotating and semi-stationary multi-beamline architecture study for cardiac CT imaging. , 2014, , .		1
395	Low-field designs for interior MRI and CT coupling. , 2015, , .		1
396	Sinogram-based attenuation correction in PET/CT. Journal of X-Ray Science and Technology, 2016, 24, 9-22.	1.0	1

#	Article	IF	CITATIONS
397	Innovation and fusion of x-ray and optical tomography for mouse studies of breast cancer. Proceedings of SPIE, 2016, , .	0.8	1
398	Characteristic performance investigation of a photon counting detector for x-ray fluorescence imaging applications. Proceedings of SPIE, 2017, , .	0.8	1
399	Initial analysis of the middle problem in CT image reconstruction. Journal of X-Ray Science and Technology, 2017, 25, 547-559.	1.0	1
400	Clinical validation of CT image reconstruction with interior tomography. Journal of X-Ray Science and Technology, 2018, 26, 303-309.	1.0	1
401	Graph Regularized Sparse Autoencoders with Nonnegativity Constraints. Neural Processing Letters, 2019, 50, 247-262.	3.2	1
402	Training artificial neurons: an introduction to machine learning. , 2019, , .		1
403	Numerical study on simultaneous emission and transmission tomography in the MRI framework. , 2017, , .		1
404	Deep learning for low-dose CT. , 2017, , .		1
405	Systematic analysis of microstructured array anode target for hard x-ray grating interferometer. , 2019, , .		1
406	Cone-beam reconstruction for Micro-CT. , 0, , .		0
407	Development of bioluminescence tomography. , 2006, 6318, 104.		0
408	Analysis of Performance Evaluation of Parallel Katsevich Algorithm for 3-D CT Image Reconstruction. , 2006, , .		0
409	Special issue on recent advances in computational techniques for biomedical imaging. Communications in Numerical Methods in Engineering, 2009, 25, 581-582.	1.3	0
410	Inverse Fourier Transform in the Gamma Coordinate System. International Journal of Biomedical Imaging, 2011, 2011, 1-16.	3.9	0
411	IEEE Access Special Section Editorial: Emerging Computed Tomography Technologies. IEEE Access, 2014, 2, 1680-1682.	4.2	0
412	High resolution 3D image reconstruction in laminar optical tomography based on compressive sensing. , 2014, , .		0
413	TOP-level designs of a hybrid low field MRI-CT system for pulmonary imaging. , 2014, , .		0
414	Total variation minimization-based multimodality medical image reconstruction. , 2014, , .		0

#	Article	IF	CITATIONS
415	Second order x-ray in-line phase-contrast imaging. , 2014, , .		0
416	Real phantom datasets for the evaluation of reconstruction algorithms at various dose conditions. , 2014, , .		0
417	Material decomposition with dual energy CT. , 2015, , .		0
418	Enhancing spatial resolution for spectral \hat{l} 4CT with aperture encoding. Proceedings of SPIE, 2016, , .	0.8	0
419	Interior tomography from differential phase contrast data via Hilbert transform based on spline functions. , 2016, 9967, .		0
420	Dictionary learning-based CT detection of pulmonary nodules. Proceedings of SPIE, 2016, , .	0.8	0
421	X-ray interior tensor tomography with 2D gratings. , 2016, , .		0
422	New contrasts for x-ray imaging and synergy with optical imaging. Proceedings of SPIE, 2017, , .	0.8	0
423	K-edge-based interior tomography. Physics in Medicine and Biology, 2018, 63, 165017.	3.0	0
424	Spectral Ct Reconstruction Via Self-Similarity In Image-Spectral Tensors. , 2019, , .		0
425	Histomorphometry of Biliary Atresia with Phase-Contrast CT Microscopy Yields Unique Insights. Radiology, 2021, 299, 611-612.	7.3	0
426	Preclinical Optical Molecular Imaging. , 2014, , 241-273.		0
427	Image correction method without gain correction in grating-based x-ray phase-contrast imaging. , 2019, , .		0
428	Smoothing L0- and L1-Norm regularizers and their relations to non-local means for CT reconstruction. , 2019, , .		0
429	Machine learning assisted interior phase contrast CT. , 2019, , .		0